Observation of a three-photon electromagnetically induced transparency in hot atomic vapor

A. S. Zibrov
Department of Physics and ITAMP, Harvard University, Cambridge, Massachusetts 02138
and Lebedev Institute of Physics, RAS, Leninsky Prospect 53, Moscow 117924, Russia

C. Y. Ye, Y. V. Rostovtsev, A. B. Matsko, and M. O. Scully
Department of Physics and Institute for Quantum Studies, Texas A&M University, College Station, Texas 77843-4242
(Received 2 November 2001; published 4 April 2002)

We demonstrate experimentally the effect of a three-photon electromagnetically induced transparency in hot ^{85}Rb atomic vapor driven by two coherent electromagnetic fields. The narrow transparency window is observed on the background of high-contrast Doppler-free subnatural absorption resonance. Our analytical calculations and numerical simulations are in good agreement with the experimental data. Both the transparency and the absorption resonances can find applications in high-precision metrology.

DOI: 10.1103/PhysRevA.65.043817 PACS number(s): 42.50.Gy, 03.67.−a, 42.65.Tg

Mediated by the effects of coherent population trapping (CPT) [1] and electromagnetically induced transparency (EIT) [2], nonlinear optical interactions can be significantly enhanced in comparison with two-level resonant systems. This was first recognized for Λ-type three-level configuration [3] and subsequently developed for a variety of multilevel systems.

In particular, a four-level *N*-type configuration displaying large nonlinearity attracts a lot of attention because of its broad range of applications in quantum and nonlinear optics [4]. This system demonstrates either an efficient self-action at a single-photon energy level [5] or strong interaction of two electromagnetic fields via refractive [6–8] and/or absorptive [9] nonlinearities. Several experimental studies of spectral properties of real *N*-type configurations have been performed quite recently [10].

Doppler-free absorption resonances that can be observed in an *N*-type level configuration represent another important feature of the system. Such resonances remove the strict restrictions on the Doppler-free geometry imposed by conventional nonlinear spectroscopy [11].

We report here an experimental observation of a new kind of strong and narrow Doppler-free absorption (up to $\sim$95%) and transmission resonances in hot rubidium vapor. We study propagation of two electromagnetic fields through isotopically pure ^{85}Rb atomic vapor. One (drive) field is redshifted from either D_1 or D_2 lines of ^{85}Rb, while the other (probe) field is nearly resonant with one of the atomic transitions. The resonances occur when the frequency difference between the drive and probe fields is equal to the hyperfine splitting of the ground state of the atom, and the probe field is tuned to the center of the Doppler-broadened atomic transition [see Fig. 1(b)]. Our numerical simulations, which take into account the relevant atomic levels [see Fig. 2(a)], are in good agreement with the experimental results.

Simplifying the problem via the adiabatic elimination of a virtual state $|\tilde{a}\rangle$, we transform the level configuration to the well-known cascade three-level scheme [Fig. 2(b)]. Using this approach, we prove analytically that the absorption and transparency resonances, observed in our experiment, can be treated as three-photon Raman-like absorption and three-photon EIT resonance, respectively.

The experimental setup and the relevant levels of ^{85}Rb are shown in Fig. 1. The probe and drive fields are indicated by dashed and solid lines, respectively. The probe radiation is tuned at the transition $5S_{1/2}$ $(F=3) \rightarrow 5P_{1/2}$ (or $5P_{3/2}$) and is characterized by Rabi frequency Ω_P. The drive radiation has Rabi frequency Ω_D and its frequency is redshifted from the corresponding transition by the amount of the ground-state hyperfine splitting $\omega_{cb}=3.035$ GHz.

The overlapped laser beams propagate to be parallel to each other. The residual divergence of the laser beams is of the order of 3×10^{-3} rad. The beams are focused into the cell by the lens with a focal length of $F=30$ cm. The extended cavity diode lasers with maximum power 12 mW (drive) and 8 mW (probe) and linewidth $\leqslant$100 kHz are used in our experiment.

The ^{85}Rb cell filled with 3 Torr of neon buffer gas is placed into a chamber with three layers of μ-metal shielding to eliminate the influence of the stray magnetic fields on our

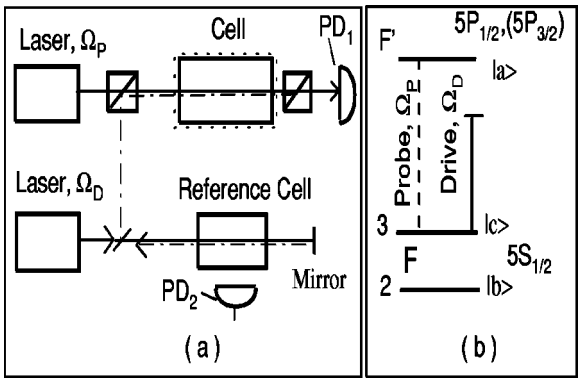

FIG. 1. (a) Experimental setup. Atomic cell contains ^{85}Rb isotope and 3 Torr of Ne. The reference cell contains a natural mixture of ^{85}Rb and ^{87}Rb isotopes. Photodiodes PD_1 and PD_2 are used to detect transmitted and scattered radiation, respectively. (b) Energy diagram of ^{85}Rb and frequency tunings of the probe Ω_P and drive Ω_D fields for which three-photon EIT resonance was observed. The frequency of the drive field Ω_D is less than the frequency of probe field Ω_P by the ground-state hyperfine splitting.

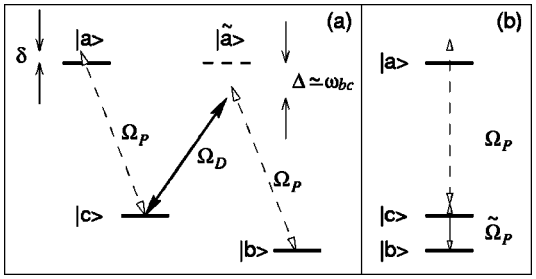

FIG. 2. (a) Effective scheme describing interaction of the electromagnetic fields and the atomic system. Because the fields are weak enough and the detuning Δ is large, the virtual level $|\tilde{a}\rangle$ is almost empty. (b) Further simplification of the scheme (a). The effective probe field is characterized by Rabi frequency $\tilde{\Omega}_P = \Omega_P \Omega_D^* / \Delta$.

measurements. The 3-cm-long cell is kept at a temperature of 62 °C which corresponds to the rubidium atomic density of 5×10^{11} cm^{-3}. The reference cell containing the natural mixture of ^{87}Rb and ^{85}Rb isotopes is used to calibrate the laser frequency. The fluorescence of rubidium atoms excited by the driving laser from the cell is detected by a photodiode PD_2.

The observed spectra are presented in Figs. 3–5. The dependence of transmission of the probe field on the frequency of the drive laser radiation is shown in Fig. 3(a) by curve *A*. The fluorescence spectrum of Rb atoms in the reference cell is shown in Fig. 3(a) by curve *B*. This spectrum has been detected by the photodiode followed by an inverted amplifier. The reference spectrum displays the resonances corresponding to the D_1 lines of ^{85}Rb and ^{87}Rb. The frequency sweeping range for the drive laser is about 8 GHz, which covers the hyperfine splitting of the rubidium ground-state. The powers of the drive and probe lasers at the entrance of the cell are equal to 10 mW and 3.2 mW, respectively.

It is instructive to distinguish the drive tuning in three particular frequency regions, denoted as "i," "ii," and "iii." The atomic-field configurations for these regions are shown in the energy-level diagrams in Fig. 3(b).

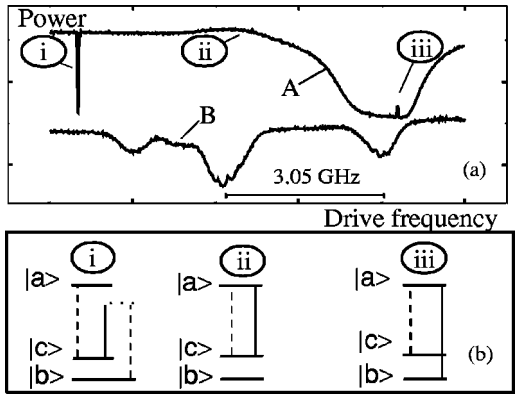

FIG. 3. (a) Curve *A* shows the *probe* field transmission versus the *drive* detuning; curve *B* shows the fluorescence in the reference cell. Absorption in region "iii" is almost 100%. (b) Tunings of the drive field for particular regions of curve *A*.

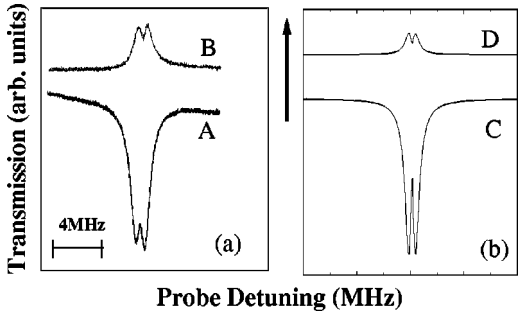

FIG. 4. The measured and calculated absorption spectra for the probe and drive fields. (a) Experiment: curve *A* is for the probe, curve *B* is for the drive. Initial powers of the probe and drive fields are equal to 5 mW and 8 mW, respectively. (b) Numerical simulations: curve *C* is for the probe, curve *D* is for the drive. We assume that Doppler linewidth (full width at half maximum) is equal to 600 MHz, the linewidth of the coherence $\gamma_{bc} = 5$ kHz, and the detuning of the driving field from the corresponding transition 3.035 GHz.

The narrow resonance in the frequency region "i" is observed when the drive frequency ν_D obeys the condition $\nu_D \approx \nu_P - \omega_{cb}$, where ν_P is the probe frequency. The maximum absorption is ~95% at this point, whereas the background Doppler-broadened absorption resonance is only ~4%. This background absorption increases up to ~21% if the drive field is off. The finding of this resonance is the main result of this paper.

The broad, nearly invisible resonance in region "ii" results from the optical pumping caused by both strong drive and probe fields tuned to the same transition $|c\rangle \rightarrow |a\rangle$. The maximum transmission of the probe field at this resonance reaches as high as 100% due to a complete depletion of the population of the upper ground state ($F = 3, 5S_{1/2}$) by both the drive and the probe fields.

The resonance in region "iii" represents the EIT effect in

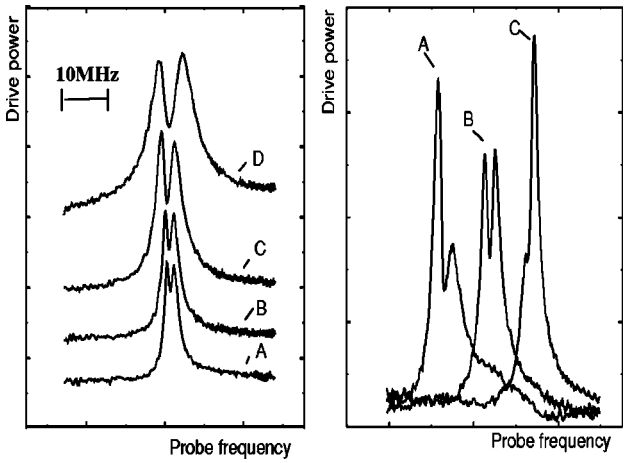

FIG. 5. (a) The three-photon resonance for the drive field at different intensities of the probe field: *A*, 0.44 W/cm^2; *B*, 0.56 W/cm^2; *C*, 0.68 W/cm^2; *D*, 1.0 W/cm^2. Drive intensity is equal to 0.8 W/cm^2, temperature of the cell 60 °C, and the angle between the laser beams 10^{-2} rad. (b) The three-photon resonance for various detunings of the drive field: curve *A*, +40 MHz; curve *B*, 0 MHz; curve *C*, −50 MHz. Probe intensity is about 1 W/cm^2.

the Doppler-broadened Λ medium. The transparency resonance results from the atomic coherence between hyperfine sublevels of the ground state induced by the applied electromagnetic fields.

The origin of the strong narrow resonance in region "i" can be interpreted in terms of the three-photon absorption process shown in Fig. 2(a) and Fig. 3(b). The first probe photon is absorbed by transferring the atom from the ground state $|b\rangle$ into an intermediate "virtual" state $|\tilde{a}\rangle$. The stimulated emission of a photon at the drive frequency occurs transferring from the "intermediate" state into state $|c\rangle$. And finally, the second probe photon is absorbed from the state $|c\rangle$ into the final state $|a\rangle$. The total "budget" of the above three-photon process indicates that two probe photons are absorbed and one photon is emitted at the drive frequency.

In addition, the atomic polarization at the transition $|a\rangle \rightarrow |b\rangle$ is induced by the above-mentioned multiphoton absorption process, and a parametric process similar to [12] should occur. Indeed, a new coherent field has been detected at the frequency $\nu_N = \nu_P + \omega_{cb}$. This field has the same polarization as that of the drive field and its power reaches $\sim 3\%$ of the probe power for high densities of atomic vapor. For low densities of atomic vapor, the new field vanishes while three-photon resonance persists. Because the amplitude of the new field is small, it does not affect significantly the population transfer from state $|a\rangle$ to state $|b\rangle$. The new field is readily observed by the transmission spectrum of the external Fabry-Perot cavity or by the beat-note signal (with the drive) at a frequency of 6.07 GHz.

Narrow three-photon resonance can be observed for the probe as well as for the drive field (Fig. 4). However, if the probe field has absorption, the drive field has amplification (transparency increase). By the term *three-photon EIT*, we mean changes in the transparency for the probe field. The linewidths of the resonances for the probe and drive fields coincide and are subnatural for moderate intensities.

A set of line shapes of the transparency resonance for the drive field as a function of the probe detuning and various probe field intensities is shown in Fig. 5(a). The Doppler-free subnatural absorption spike splits into two components when the intensity of the probe increases. Figure 5(b) presents the change of the line shapes of the resonance for various drive field frequencies.

We perform numerical simulations of the experiment. The results of the calculations are presented in Fig. 4(b). One can see that the simulations have good agreement with the experimental data. The difference between simulation and experiment may result from the inhomogeneity of laser field profiles and residual Doppler broadening because of the misalignment of laser beams. The laser beam divergence is of the order of $\delta\phi \simeq 3\times 10^{-3}$ rad, which gives residual Doppler broadening of the order $W_D \delta\phi \simeq 1$ MHz, where W_D is the Doppler linewidth. The width is much less than the width of the observed structure, thus it does not have an influence on the total width but on the resolution of fine details such as the dip between the peaks.

To explain the experimental results, let us perform here simplified analytical calculations by introducing the virtual level $|\tilde{a}\rangle$, as shown in Fig. 2(a). Using the fact that the detuning for the drive laser is very large even in terms of Doppler width, we can eliminate this level by using adiabatic transformation, as per [13]. Finally, we transform the scheme into an effective cascade configuration [Fig. 2(b)] that is described by an effective Hamiltonian

$$H = \hbar\left(\delta + \frac{|\Omega_D|^2 - |\Omega_P|^2}{\Delta}\right)|c\rangle\langle c| + \hbar\left(2\delta - \frac{|\Omega_D|^2 + |\Omega_P|^2}{\Delta}\right)|a\rangle\langle a| + \hbar\left(\frac{\Omega_D^* \Omega_P}{\Delta}|c\rangle\langle b| + \Omega_P |a\rangle\langle c| + adj.\right). \quad (1)$$

The steady-state propagation of the electromagnetic fields obeys the Maxwell equations

$$\frac{\partial \Omega_P}{\partial z} = i\kappa\left\langle \rho_{ac} + \frac{\Omega_D}{\Delta}\rho_{cb} - \frac{\Omega_P}{\Delta}(\rho_{cc} + \rho_{aa})\right\rangle_v, \quad (2)$$

$$\frac{\partial \Omega_D}{\partial z} = i\kappa\left\langle \frac{\Omega_P}{\Delta}\rho_{bc} + \frac{\Omega_D}{\Delta}(\rho_{cc} - \rho_{aa})\right\rangle_v, \quad (3)$$

where δ is the probe detuning from transition $|c\rangle \rightarrow |a\rangle$, Δ is the probe detuning from transition $|b\rangle \rightarrow |a\rangle$, $\kappa = 3N\lambda^2\gamma/(8\pi)$, γ is the radiative decay rate of the level $|a\rangle$, $\langle \cdots \rangle_v = \int dv(\cdots)/\{\pi[1 + (v/v_T)^2]\}$ stands for averaging over Doppler distribution [14], v_T is the averaged thermal atomic velocity, and ρ_{ij} are the matrix elements resulting from the solution of the Bloch equations generated by Hamiltonian H in Eq. (1).

Let us find properties of the EIT window in the case of sufficiently weak fields $|\Omega_D| \gg |\Omega_P|, \Delta\gamma_{bc} > |\Omega_D||\Omega_P|$, where γ_{bc} is the homogeneous decay rate of the low-frequency atomic coherence ($\gamma \gg \gamma_{bc}$). This decay is determined by the time of flight of atoms through the atomic beam and by the divergence of the laser beams. We assume that almost all of the atomic population is in the state $|b\rangle$, so $\rho_{bb} \approx 1$. Then the field propagation is determined by the long-lived atomic coherence ρ_{cb}. The steady-state solution of the Bloch equation gives

$$\langle \rho_{cb} \rangle_v = i\frac{\Omega_D^* \Omega_P}{\Delta} \times \frac{\gamma + W_D + i\left(2\delta - \frac{|\Omega_D|^2}{\Delta}\right)}{\left[\gamma + W_D + i\left(2\delta - \frac{|\Omega_D|^2}{\Delta}\right)\right]\left[\gamma_{bc} + i\left(\delta + \frac{|\Omega_D|^2}{\Delta}\right)\right] + |\Omega_P|^2}, \quad (4)$$

where $W_D = \nu_P v_T / c$ is the Doppler linewidth.

Equation (4) resembles a usual solution for the transparency window for the case of EIT in a cascade configuration having a weak probe field $\tilde{\Omega}_P = \Omega_D^* \Omega_P / \Delta$ and a strong field Ω_P. The difference from the usual EIT solution arises due to ac Stark shifts that modify the field detunings. The center of the EIT window is observed at $\delta \approx -|\Omega_D|^2/\Delta$. The width of the EIT structure is $\sim |\Omega_P|^2 / W_D$.

It is worth mentioning that, in the cascade configuration, both optical transitions $|b\rangle \rightarrow |c\rangle$ and $|c\rangle \rightarrow |a\rangle$ are Doppler-broadened. The narrow EIT spike can be observed if the two-photon transition $|b\rangle \rightarrow |a\rangle$ is Doppler-free. This is possible if the fields applied to transitions $|b\rangle \rightarrow |c\rangle$ and $|c\rangle \rightarrow |a\rangle$ are counterpropagating and the frequencies of the fields nearly coincide. In our case, the microwave transition $|b\rangle \rightarrow |c\rangle$ is Doppler-free if the probe and drive fields propagate in the same direction. The other transitions are Doppler-broadened. This indicates a significant difference between our configuration and the usual cascade configuration.

In conclusion, we observe a new kind of Doppler-free subnatural absorption and transparency resonances in a non-Doppler-free geometry. This rather contraintuitive result demonstrates an important role of quantum coherence in optics. The coherence results in the extension of the possible applications of hot atomic vapors by eliminating Doppler broadening without cooling. For example, this effect might be employed to enhance gain of gas lasers (with or without population inversion), or to obtain a high index of refraction without absorption. The narrow subnatural width of the resonances could be very useful in quantum computing. The three-photon transparency resonance inherits the properties of the regular EIT resonance but has one significant advantage in comparison with usual EIT: It has almost no Doppler background. This unique feature is important for different applications such as atomic clocks and magnetometry.

This work was supported by the Office of Naval Research, the Welch Foundation, the Texas Advanced Research and Technology Program, the U.S. Air Force, and DARPA. The authors are grateful for T. Zibrova's assistance with the semiconductor lasers. A.S.Z. appreciates valuable discussions with M. D. Lukin.

[1] For reviews on CPT, see E. Arimondo, in *Fundamentals of Quantum Optics III*, edited by F. Ehlotzky, Lecture Notes in Physics Vol. 420 (Springer, Berlin, 1993), p. 170; E. Arimondo, in *Progress in Optics*, edited by E. Wolf (Elsevier, Amsterdam, 1996), Vol. 35, p. 257.

[2] For reviews on EIT, see S.E. Harris, Phys. Today **50** (7), 36 (1997); J.P. Marangos, J. Mod. Opt. **45**, 471 (1998).

[3] S.E. Harris, J.E. Field, and A. Imamoglu, Phys. Rev. Lett. **64**, 1107 (1990).

[4] M.D. Lukin and A. Imamoglu, Nature (London) **413**, 273 (2001).

[5] A. Imamoglu, H. Schmidt, G. Woods, and M. Deutsch, Phys. Rev. Lett. **79**, 1467 (1997); S. Rebic, S.M. Tan, A.S. Parkins, and D.F. Walls, J. Opt. B: Quantum Semiclassical Opt. **1**, 490 (1999); K.M. Gheri, W. Alge, and P. Grangier, Phys. Rev. A **60**, 2673 (1999); A.D. Greentree, J.A. Vaccaro, S.R. de Echaniz, A.V. Durrant, and J.P. Marangos, J. Opt. B: Quantum Semiclassical Opt. **2**, 252 (2000).

[6] H. Schmidt and A. Imamoglu, Opt. Lett. **21**, 1936 (1996).

[7] S.E. Harris and L.V. Hau, Phys. Rev. Lett. **82**, 4611 (1999).

[8] M.D. Lukin and A. Imamoglu, Phys. Rev. Lett. **84**, 1419 (2000).

[9] S.E. Harris and Y. Yamamoto, Phys. Rev. Lett. **81**, 3611 (1998).

[10] B.S. Ham and P.R. Hemmer, Phys. Rev. Lett. **84**, 4080 (2000); V.M. Entin, I.I. Ryabtsev, A.E. Boguslavskii, and I.M. Beterov, JETP Lett. **71**, 175 (2000); M. Yan, E.G. Rickey, and Y. Zhu, Opt. Lett. **26**, 548 (2001); M. Yan, E.G. Rickey, and Y. Zhu, Phys. Rev. A **64**, 041801 (2001); S.R. de Echaniz, A.D. Greentree, A.V. Durrant, D.M. Segal, J.P. Marangos, and J.A. Vaccaro, *ibid.* **64**, 013812 (2001).

[11] A.K. Popov and V.M. Shalaev, Phys. Rev. A **59**, 946 (1999); C. Y. Ye, A. S. Zibrov, Y. V. Rostovtsev, and M. O. Scully, Phys. Rev. A **65**, 043805 (2002).

[12] M.D. Lukin, M. Fleischhauer, A.S. Zibrov, H.G. Robinson, V.L. Velichansky, L. Hollberg, and M.O. Scully, Phys. Rev. Lett. **79**, 2959 (1997); V.A. Sautenkov, M.M. Kash, V.L. Velichansky, and G.R. Welch, Laser Phys. **9**, 889 (1999).

[13] S.E. Harris, Opt. Lett. **19**, 2018 (1994).

[14] To simplify analytical calculations, we use the Lorentzian distribution function instead of the Gaussian.